Investigation of estimator algorithms for high speed drive systems

Péter Stumpf
Department of Automation and Applied Informatics
Budapest University of Technology and Economics
Budapest, Hungary
stumpf@aut.bme.hu

Ádám Lajos Váradi
Department of Automation and Applied Informatics
Budapest University of Technology and Economics
Budapest, Hungary

***Abstract*—In high speed drives both the sampling over reference frequency ratio F and the carrier over reference frequency m_f is a low value. The low m_f ratio results voltage and current harmonic spectra far more unfavorable than at standard ratios. The low F ratio can result uncertainty and inaccuracy in the calculation of the magnitude and angle of stator or rotor flux vector or in the estimation of the actual value of the speed.**

The current paper derives the discrete equations of different flux and speed estimator algorithms by using Tustin approximation. The performance of the algorithms, both in open and closed loop, is demonstrated via numerical simulation using a high speed motor drive with a low sampling to fundamental frequency ratio.

***Keywords*—Induction machine, Estimator, High speed drives, Discretization**

I. Introduction

Nowadays increasing attention has been paid to high speed induction and permanent magnet sychronous machines [1]. The high rated fundamental frequency f_1 (from few hundred up to thousand Hz) and the limited carrier (switching) frequency f_c ($\leq 15-25$ kHz) result in low $m_f = f_c/f_1$ frequency ratios (usually $m_f < 21$). The low frequency ratios result in a far more unfavorable stator voltage, flux and current harmonic spectra that obtained at high frequency ratios.

In modern closed loop controlled high speed drive systems, all the signal processes including the speed and current regulation loop and also the PWM block are implemented in the digital domain. Even with the up-to-date digital devices with clock frequency in the range of tens of MHz, the sampling frequency (f_s) is limited. Its outcome is that the ratio of the sampling frequency and the actual fundamental frequency $F = f_s/f_1$ around the maximum speed of a high speed motor is also low, resulting in stability problems and sampling error in the regulation loop.

Therefore, the low F ratio is a source of possible error in digitally controlled drives. In recent years drives with low F ratio have gained more attention and have been analyzed in research papers [2]–[5]. To improve the available flux and speed estimator techniques for induction machines an adequate discrete estimation methodology should be found. In this way, high speed drives with low F ratio can provide robust, reliable and high dynamic performance similar to standard drives with high F ratio.

The goal of the paper is to derive the discrete recursive equations of different flux and speed estimator algorithms and analyze their performance for different F ratio values and for machine parameter sensitivity.

II. Theoretical background

The squirrel cage induction machine in a rotating reference frame $d-q$, which rotates with an arbitrary selected ω_R angular speed, can be described by the following two differential equations expressing the stator and rotor voltage balance

$$\mathbf{v}_s = R_s\mathbf{i}_s + \frac{d\mathbf{\Psi}_s}{dt} + j\omega_R\mathbf{\Psi}_s \tag{1}$$

$$\mathbf{v}_r = R_r\mathbf{i}_r + \frac{d\mathbf{\Psi}_r}{dt} - j(\omega_R-\omega)\mathbf{\Psi}_r = \mathbf{0} \tag{2}$$

and by the stator $\mathbf{\Psi}_s$ and rotor $\mathbf{\Psi}_r$ flux relations

$$\mathbf{\Psi}_s = L_s\mathbf{i}_s + L_m\mathbf{i}_r \tag{3}$$

$$\mathbf{\Psi}_r = L_m\mathbf{i}_s + L_r\mathbf{i}_r, \tag{4}$$

where ω is the mechanical angular speed. R_s and R_r are the resistance in one stator and rotor phase, respectively. The total inductance of the stator and rotor can be given as $L_s = L_m + L_{ls}$ and $L_r = L_m + L_{lr}$, where L_{ls} and L_{lr} denote the leakage inductance of the stator and rotor.

A. Flux estimators

In closed loop vector control of induction machines it is essential to obtain the magnitude and the actual angle of the rotor flux. Due to the complexities and lack of mechanical robustness of the airgap flux measurement, the stator and rotor flux is estimated by real-time calculations. Many flux estimator and observer techniques have been developed over the years [3], [6]–[8]. Most of them use the measured stator current and the applied stator voltage vector to calculate the rotor flux.

1) Flux observer based on the stator voltage: In stationary reference frame ($\omega_R = 0$) the stator flux vector can be easily obtained by integrating the difference between stator voltage and the voltage drop across the stator resistance. From the stator flux vector the rotor flux vector can be calculated directly. The equations are as follows

$$\frac{d\mathbf{\Psi}_s}{dt} = \mathbf{v}_s - R_s\mathbf{i}_s \tag{5}$$

$$\mathbf{\Psi}_r = \frac{L_r}{L_m}\left(\mathbf{\Psi}_s - \sigma L_s\mathbf{i}_s\right) \tag{6}$$

This paper was supported by the János Bolyai Research Scholarship of the Hungarian Academy of Sciences. Research supported by the National Research, Development and Innovation Office (NKFIH) under the grant FK 124913.

.

The main drawback of the method is that it applies an open-loop integrator. In practical application, to improve and stabilize the performance, a feedback path is often used [6].

Figure 1(a) presents the block diagram of this method.

2) Flux observer based on stator current: By selecting the angular speed of rotating reference frame to be the mechanical angular speed $\omega_R = \omega$, (1)-(4) can be simplified as

$$\frac{d\mathbf{\Psi}_r}{dt} = \frac{R_r L_m}{L_r}\mathbf{i}_s - \frac{R_r}{L_r}\mathbf{\Psi}_r \tag{7}$$

$$\mathbf{\Psi}_s = \sigma L_s \mathbf{i}_s + \frac{L_m}{L_r}\mathbf{\Psi}_r, \tag{8}$$

where $\sigma = 1 - \frac{L_m^2}{L_r L_s}$. This method has the advantage over the previous one, that it applies a closed-loop integrator. However, it requires the mechanical angle for coorindate transformation. Figure 1(b) shows the block diagram of this current model.

3) Gopinath estimator: Gopinath estimator combines the flux estimation based on the stator voltage and stator current. The rotor flux vector calculated by the voltage model is subtracted from the rotor flux calculated by the current model. The difference is forced to zero by a PI type controller. The output of the PI controller is added to the input stator voltage vector as

$$\frac{d\mathbf{\Psi}_s}{dt} = \mathbf{v}_s + \mathbf{v}_{PI} - R_s \mathbf{i}_s \tag{9}$$

Its block diagram can be seen on Fig.1(c).

As it will be demonstrated later on, this observer is able to perform well even when the sampling over reference frequency ratio F and the carrier over reference frequency m_f is a low value. Furthermore, it is robust against parameter uncertainties.

B. Speed estimators

The actual value of the mechanical speed is required to control the speed of the drive or to calculate the flux using stator current based or Gopinath stlye flux observer. The mechanical speed sensors, attached to the machines shaft, increase the overall cost. Furthermore, in the case of high speed drives, it is very hard and expensive to find a speed sensor, which provides good accuracy from zero speed up to rated speed. By using speed estimator the mechanical speed sensor can be avoided.

1) Current based MRAS: Model Reference Adaptive System (MRAS) observers are widely used to calculate the mechanical speed of the induction machine. MRAS observes consist of a reference model and an adaptive or adjustable model, which is the function of the estimated variable. The difference between the two models is evaluated by an adaptation mechanism. This mechanism, generally a PI-type controller, forces the difference between the two models to be zero [9].

In the so-called current based (CB) MRAS observer [7], the induction motor is used as a reference system. The flux estimator based on stator current together with a current estimator form the adaptive model (Fig.2(a)).

In stationary reference frame ($\omega_R = 0$) the stator current can be estimated by using (1)-(4) as

$$\mathbf{i}_{s,est} = \frac{1}{\sigma L_s}\int \mathbf{v}_s - \left(R_s + \frac{L_m^2 R_r}{L_r^2}\right)\mathbf{i}_{s,est} - \frac{L_m}{L_r} j\omega \mathbf{\Psi}_r + ... + \frac{L_m R_r}{L_r^2}\mathbf{\Psi}_r \quad dt, \tag{10}$$

where the subscript est referes to "estimated". As it can be seen, the current esimator needs the rotor flux, which can be obtained from the flux estimator based on the stator current.

The adaptation mechanism uses the following equations

$$\zeta = (i_{s\alpha} - i_{s\alpha,est})\Psi_{r\beta} + (i_{s\beta} - i_{s\beta,est})\Psi_{r,\alpha} \tag{11}$$

$$\omega_{est} = K_P \zeta + K_I \int_0^t \zeta dt, \tag{12}$$

where α and β denote the real and imaginary components of the vectors in the stationary reference frame. K_P and K_I are the gains of the PI controller. It should be noted, CB-MRAS provides not only the mechanical speed, but thanks to the flux observer part the rotor flux vector as well.

In the literature other MRAS observer techniques are also analyzed. Paper [9] compares the so called reference frame (RF) MRAS with the CB-MRAS. A model predictive MRAS speed estimator based on the finite control set-model principle is introduced in [8]. Its advantage is that, it eliminates the need for the PI type controller.

2) PLL-type estimator: A simpler method to estimate the mechanical speed as well as the electrical angle ρ_{est} is based on the calculation of the Back Electro Motive Force (BEMF) later denoted by vector $\mathbf{e}$. It can calculated in the stationary reference frame ($\omega_R = 0$) as

$$\mathbf{e_{est}} = \mathbf{v}_s - R_s \mathbf{i}_s - \sigma L_s \frac{d\mathbf{i}_s}{dt} \tag{13}$$

After this, $\mathbf{e}$ should to be transformed to a rotating reference frame ($\omega_R = \omega_1$) with the estimated electrical angle ρ_{est}. Furthermore, it is assumed that the real axis is aligned with the rotor flux vector ($\mathbf{\Psi} = \Psi_d = \Psi$). In this field oriented coordinate system $\mathbf{e}$ is leading by $90°$ the rotor flux $\mathbf{\Psi}_r$ in steady-state, so its real d axis component should be zero as

$$e_d = \frac{L_m}{L_r}\frac{d\Psi_d}{dt} \tag{14}$$

$$e_q = \frac{L_m}{L_r}\omega_{1,est}\Psi \tag{15}$$

From the latter equation ω_1 can be calculated theoretically as

$$\omega_{1,est} = \frac{L_r}{L_m \Psi} e_q \tag{16}$$

Error in the estimation generates a non-zero d axis component of the BEMF. The larger the value $e_{d,est}$, the larger the error is. It can be corrected as

$$\omega_{1,est} = \frac{L_r}{L_m \Psi_r}\left(e_{q,est} - \underbrace{sqn(e_{q,est})e_{d,est}}_{\text{correction}}\right) \tag{17}$$

By integrating $\omega_{1,est}$ the estimated electrical angle ρ_{est} can be obtained.

The compensation forces e_d to be zero, in this way forces the estimated electric angle ρ_{est} to be the same as the real one. This behaviour is similar to a PLL method.

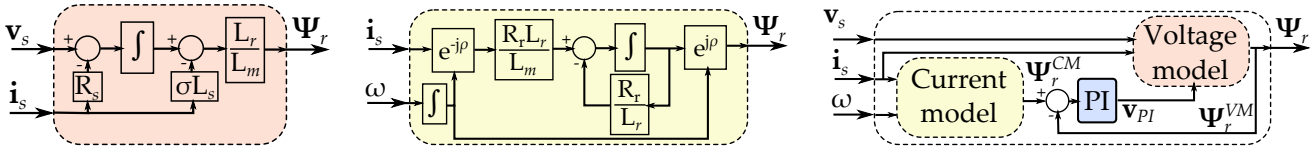

(a) Flux observer based on stator voltage (b) Flux observer based on stator current (c) Gopinath estimator

Fig. 1. Flux estimators

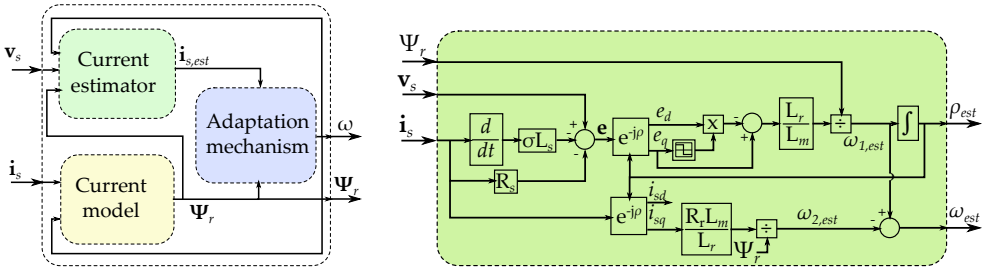

(a) CB-MRAS (b) PLL-type

Fig. 2. Speed estimators

The mechanical speed can be calculated from $\omega_{1,est}$ as

$$\omega_{est} = \omega_{1,est} - \omega_{2,est} = \omega_{1,est} - \frac{R_r L_m}{L_r} \frac{1}{\Psi_r} i_{sq} \tag{18}$$

where $\omega_{2,est}$ is the slip speed, which can obtained from (1)-(4) by assuming $\omega_R = \omega_1$ and steady-state condition for the stator and rotor fluxes (their derivatives are zero).

Figure 2(b) presents the block diagram of the PLL based speed estimator.

It should be noted, in the case of the PLL based estimator, the magnitude of the rotor flux Ψ_r is an input value. It can be assumed to be constant and equal to its rated value, or it can be calculated by using one of the flux observer presented previously.

III. Discretization using Tustin Approximation

In modern high-performance closed loop drive systems, all signal processes including the processes in speed and the current regulation loop and also the PWM block are implemented in the digital domain. The signal flow of the estimator algorithms presented in the previous section in the continuous time domain has to be discretized by sampling.

The applied discretization technique has a great importance on the performance, therefore the selection of the approximation method plays a crucial role.

Paper [2] introduces a power series approximation for real time implementations of a discrete flux observer. Different numerical integration methods for discretization of the current based MRAS estimator are compared in [5]. A modified Euler approximation is used to discretize flux estimation is presented in [4].

In the current paper, to obtain a more accurate and stable flux or speed estimation the so-called trapezoidal (Tustin) integral approximation was used. It increases the computational complexity, but it provides stable performance. Today processors with capability of calculation of complex algorithm using floating point arithmetic are available even at low cost.

The Tustin or bilinear approximation provides the best frequency-domain match between the continuous and discretized systems.

By applying Tustin approximation, the discrete integral can be calculated as follows between two consecutive time steps

$$f((k+1)T_s) - f((k)T_s) = \int_{kT_s}^{(k+1)T_s} g(\tau)d\tau, \tag{19}$$

where T_s is the sampling period.

A. Flux observer based on stator current

It should be noted, this observer can estimate the present value of the rotor flux in the kth period and it cannot be used to estimate the next sample as it has no advanced information for accomplishing this [6]. Therefore (19) should be calculated between $(k-1)Ts$ and kT_s instants.

Using (7)

$$\mathbf{\Psi}_r(kT_s) - \mathbf{\Psi}_r((k-1)T_s) = \frac{R_r L_m}{L_r} \int_{(k-1)T_s}^{kT_s} \mathbf{i}_s(\tau)d\tau - \frac{R_r}{L_r} \int_{(k-1)T_s}^{kT_s} \mathbf{\Psi}_r(\tau)d\tau \tag{20}$$

The sinusoidal stator current viewed in the RRF appears to be a slow moving sinusoidal signal at the slip frequency and can be modelled as a ramp signal with an average value of $(\mathbf{i}_s(kT_s) + \mathbf{i}_s((k-1)T_s))/2$.

The flux integral is approximated with the trapezoid according to Tustin definition as

$$\int_{(k-1)T_s}^{kT_s} \mathbf{\Psi}_r(\tau)d\tau = \frac{T_s}{2}\Big(\mathbf{\Psi}_r(kT_s) + \mathbf{\Psi}_r((k-1)T_s)\Big) \tag{21}$$

The discrete version of the flux estimator

$$\mathbf{\Psi}_r(kT_s) = K_1\mathbf{\Psi}_r((k-1)T_s) + K_2(\mathbf{i}_s(kT_s) + \\ + \mathbf{i}_s((k-1)T_s)) \quad (22)$$

where

$$K_1 = \frac{1-\frac{R_rT_s}{2L_r}}{1+\frac{R_rT_s}{2L_r}} \quad \text{and} \quad K_2 = \frac{\frac{R_rL_mT_s}{2L_r}}{1+\frac{R_rT_s}{2L_r}} \quad (23)$$

B. Flux observer based on stator voltage

This type of observer inherently estimates the next sample instant. Thus

$$\mathbf{\Psi}_s((k+1)T_s) - \mathbf{\Psi}_s(kT_s) = \int_{kT_s}^{(k+1)T_s} \mathbf{v}_s(\tau)d\tau \\ - R_s \int_{kT_s}^{(k+1)T_s} \mathbf{i}_s(\tau)d\tau \quad (24)$$

By assuming $\mathbf{v}_s$ is constant during sampling period ($\mathbf{v}_s(\tau) = \mathbf{v}_s(kT_s)$, $T_s \leq \tau < (k+1)T_s$), the discrete form of (5) and (6) can be written as

$$\mathbf{\Psi}_s((k+1)T_s) = \mathbf{\Psi}_s(kT_s) + T_s\mathbf{v}_s(kT_s) + \frac{T_s}{2}\big(\mathbf{i}_s(kT_s) \\ + \mathbf{i}_s((k+1)T_s)\big) \quad (25)$$

$$\mathbf{\Psi}_r((k+1)T_s) = \frac{L_r}{L_m}\big(\mathbf{\Psi}_s((k+1)T_s) + \sigma L_s\mathbf{i}_s((k+1)T_s)\big) \quad (26)$$

As it can be seen, to avoid lagging response, the value of the stator current in the $(k+1)^{th}$ period is required. As it is not available, it should be estimated by (10).

C. Gopinath estimator

The Gopinath estimator combines the flux estimation based on the stator voltage and stator current. In the Gopinath estimator the estimated rotor flux vector $\mathbf{\Psi}_r(kT_s)$ based on the stator current is calculated first using (22). After this, a discrete PI controller, using Tustin approximation, forces the error between the $\mathbf{\Psi}_r(kT_s)^{SC}$ (calculated based on the stator current (SC)) and $\mathbf{\Psi}_r(kT_s)^{SV}$ (calculated by the voltage model using (26) in the previous sampling period) to be zero.

The $\mathbf{v}_{PI}(kT_s)$ output of the controller is used to estimate the stator flux as follows (see (25) and (9))

$$\mathbf{\Psi}_s((k+1)T_s) = \mathbf{\Psi}_s(kT_s) + T_s\big(\mathbf{v}_s(kT_s) + \mathbf{v}_{PI}(kT_s)\big) \\ + \frac{T_s}{2}\big(\mathbf{i}_s(kT_s) + \mathbf{i}_s((k+1)T_s)\big) \quad (27)$$

$\mathbf{\Psi}_r((k+1)T_s)$ can be calculated using (26). However, as it was mentioned previously, the estimated value of $\mathbf{i}_s((k+1)T_s)$ is required in (26) and (27).

Current estimator using Tustin approximation: The stator current in the $(k+1)^{th}$ period can be estimated by using (10) and (19) as

$$\mathbf{i}_{s,est}((k+1)T_s) - \mathbf{i}_{s,est}(kT_s) = \frac{1}{\sigma L_s}\int_{kT_s}^{(k+1)T_s} \mathbf{v}_s(\tau)d\tau \\ - \frac{R_e}{\sigma L_s}\int_{kT_s}^{(k+1)T_s} \mathbf{i}_{s,est}(\tau)d\tau - \frac{L_m}{\sigma L_rL_s}\int_{kT_s}^{(k+1)T_s} j\omega(\tau)\mathbf{\Psi}_r(\tau)d\tau \\ + \frac{L_mR_r}{\sigma L_r^2L_s}\int_{kT_s}^{(k+1)T_s} \mathbf{\Psi}_r(\tau) \quad (28)$$

where $R_e = R_s + \frac{L_m^2R_r}{L_r^2}$. It can be assumed, the mechanical speed and the value of the stator voltage are constant over one sampling period ($\mathbf{v}_s(\tau) = \mathbf{v}_s(kT_s)$, $\omega(\tau) = \omega(kT_s), kT_s \leq \tau < (k+1)T_s$). The flux integral can be approximated with the trapezoid according to Tustin definition as

$$\int_{kT_s}^{(k+1)T_s} \mathbf{\Psi}_r(\tau)d\tau = \frac{T_s}{2}\Big(\mathbf{\Psi}_r(kT_s) + \mathbf{\Psi}_r((k+1)T_s)\Big) \quad (29)$$

There is no advanced information on the value of $\mathbf{\Psi}_r((k+1)T_s)$. However, it can be assumed, the amplitude of the rotor flux is constant over one period as the time constant of the rotor flux is considerably higher than the sampling time. Therefore $\mathbf{\Psi}_r((k+1)T_s)$ can be estimated as

$$\mathbf{\Psi}_r((k+1)T_s) = \mathbf{\Psi}_r(kT_s)e^{j\omega_1T_s} \approx \mathbf{\Psi}_r(kT_s)e^{j\omega T_s} \quad (30)$$

as for high speed drives the slip speed is small comparing to the fundamental angular frequency and $\omega_1 \approx \omega$ (and assuming that the number of pole pairs is 1).

To stabilize the current estimator algorithm, an additional PI controller is used, which forces the difference between the measured and the estimated stator current to be zero [6]. The input of the PI controller is the error signal $\mathbf{i}_s(kT_s) - \mathbf{i}_{s,est}(kT_s)$, where $\mathbf{i}_{s,est}(kT_s)$ is the estimated stator current calculated in the previous sampling period. The $\mathbf{v}_{PI,is}(kT_s)$ output of the PI controller is added to the $\mathbf{v}_s(kT_s)$ in (28).

In summary, the stator current vector in the $(k+1)^{th}$ sampling period can be estimated as

$$\mathbf{i}_{s,est}((k+1)T_s) = K_{1C}(\mathbf{v}_s(kT_s) + \mathbf{v}_{PI,is}(kT_s)) + \\ + K_{2C}\mathbf{i}_{s,est}(kT_s) - j\omega K_{3C}\mathbf{\Psi}_r(kT_s)\big(1+e^{j\vartheta}\big) + \\ + K_{4C}\mathbf{\Psi}_r(kT_s)\big(1+e^{j\vartheta}\big) \quad (31)$$

where $\mathbf{\Psi}_r(kT_s)$ is the rotor flux calculated in the previous sampling period using (27) and

$$K_{1C} = \frac{\frac{T_s}{\sigma L_s}}{1+\frac{R_eT_s}{2\sigma L_s}} \quad K_{2C} = \frac{1-\frac{R_eT_s}{2\sigma L_s}}{1+\frac{R_eT_s}{2\sigma L_s}}$$

$$K_{3C} = \frac{\frac{L_mT_s}{2\sigma L_rL_s}}{1+\frac{R_eT_s}{2\sigma L_s}} \quad K_{4C} = \frac{\frac{L_mR_rT_s}{2\sigma L_r^2L_s}}{1+\frac{R_eT_s}{2\sigma L_s}}$$

and $\vartheta = \omega T_s$.

It should be noted, in [6] a method based on Euler approximation is introduced to estimate the stator current. Based on our experience using Tustin approximation and estimating $\mathbf{\Psi}_r((k+1)T_s)$ by (30), a much more robust and stable performance can be obtained even at low F ratios.

The advantage of Gopinath estimators is that, it can estimate the rotor flux vector valid in the next sample, thus removes the computational delay and it can improve the closed loop performance of the drive.

D. Current based MRAS

The discrete version of the CB-MRAS combines the discrete flux estimator based on stator current with a discrete current estimation.

The equation of the discrete flux estimator is given in (22). The only difference is that, the estimated mechanical speed $\omega_{est}((k-1)T_s)$, calculated in the previous sampling period, is used for coordinate transformation.

The discrete current estimator algorithm is similar to the one, which was presented previously. However, the flux estimator based on stator current can provide the present value of Ψ_r, which is valid in the the kth period. Therefore, the (28) should be discretized by Tustin method between the $(k-1)Ts$ and kT_s sampling instants. It results that, there is no need to estimate Ψ_r in the $k+1$ period using (30). Furthermore, there is no need for the additional PI controller used in the current estimation as the adaptation algorithm of the MRAS forces the estimated current to be the same as the measured one.

The discrete version of the current estimator used in CB-MRAS can be given as

$$\begin{aligned}\mathbf{i}_{s,est}(kT_s) &= K_{1C}\mathbf{v}_s(kT_s) + K_{2C}\mathbf{i}_{s,est}((k-1)T_s)\\ &- j\omega_{est}((k-1)T_s)K_{3C}\big(\mathbf{\Psi}_r(kT_s) + \mathbf{\Psi}_r((k-1)T_s)\big)+\\ &+ K_{4C}\big(\mathbf{\Psi}_r(kT_s) + \mathbf{\Psi}_r((k-1)T_s)\big) \qquad (32)\end{aligned}$$

The discrete inputs signal of the adaptation mechanism (PI controller) by using (11)

$$\begin{aligned}\zeta(kT_s) =& \big(i_{s\alpha}(kT_s) - i_{s\alpha,est}(kT_s)\big)\Psi_{r\beta}(kT_s)\\ &+ \big(i_{s\beta}(kT_s) - i_{s\beta,est}(kT_s)\big)\Psi_{r,\alpha}(kT_s) \qquad (33)\end{aligned}$$

The discrete PI controller outputs $\omega_{est}(kT_s)$.

To obtain a stable behaviour with CB-MRAS, the K_P and K_I gains of the PI controller should be selected to be large values. Based on our findings, it is worth to use variable gain K_P, and change its parameter as the function of the error signal. In this way the unwanted oscillations can be reduced.

E. PLL-type estimator

One of the advantages of the PLL-type speed estimator is its simple structure. The discrete version of the BEMF estimation (see (13)) can be written as

$$\begin{aligned}\mathbf{e_{est}}(\mathbf{kT_s}) &= \mathbf{v}(kT_s) - R_s\mathbf{i}_s(kT_s) - ...\\ &-\sigma L_s\frac{\mathbf{i}_s(kT_s) - \mathbf{i}_s((k-n)T_s)}{nT_s} \qquad (34)\end{aligned}$$

As the discrete derivative can result in additional noise, the value of the $\mathbf{e_{est}}$, after the coordinate transformation, should be filtered.

Deriving the discrete equations of the rest of the estimator algorithm based on Fig.2(b) is straightforward.

F. Compensation of frequency warping phenomena

In the case of trapezoidal type of discretization, frequency warping phenomena should be expected [10]. This phenomena cannot be neglected at low F ratio. It can be compansated by scaling the synchronous speed ω_1 in the equations of the estimator algorithms with a gain k, which can be calculated as

$$k = \frac{\omega_1 T_s}{2}\frac{1}{\tan(\omega_1 T_s/2)} \qquad (35)$$

As the slip frequency is very small, the same gain k can be used for scaling the mechanical speed ω in the equations as well (and assuming that the number of pole pairs is 1).

IV. Digital implementation

A. Sequence of current sampling and calculations

By using carrier based PWM techniques, like SVM as in the current paper, the stator phase currents are synchronously sampled twice at the negative and positive peaks of the carrier signal (see Fig.3) [11]. In this way it can be ensured that, the current is measured in the middle of the zero vector times. In ideal case it provides ripple-free feedback signals for the controllers.

The drawback of the solution is that, the sampling frequency is limited and the delay caused by the PWM peripheral (see later) introduces a phase lag limiting the achievable control bandwidth and deteriorating the performance of the control loop. In general-purpose ac drive applications this effect can be neglected, but it can be crucial, when both the sampling over fundamental frequency ratio F and the carrier over fundamental frequency m_f is low.

It should be noted, in practical drives, the lockout time, the delays of the anti-aliasing filters or the motor cable length can cause additional noise in the current signals even if they are synchronously sampled. Paper [12] introduces a method to avoid these unwanted effects.

In a processor (μC or DSP) based system after the sampling and the conversion of the phase currents an interrupt service routine (abbreviated as ISR) is called (Fig.3). In this routine the discrete version of the estimator and the controller algorithms can be found. The controller, based on the measured and the estimated signals, generates the output reference voltage $\mathbf{v}_s$ for the induction machine. The PWM algorithm, Space Vector Modulation in our case, calculates the reference signals for each phase. They are latched into the Compare Registers (CR) of the PWM peripheral of the processor to generate the switching signals.

As it was shown previously, estimator algorithms, except for the flux observer based on the stator current, use the value of the stator voltage vector $\mathbf{v}_s$ (in stationary reference frame). In practical applications, the phase voltages are not measured for simplicity and the value of the calculated reference voltage vector is used by estimators.

The sampling of the current signals, the calculation of the estimator algorithm, the control and the PWM algorithm

take less time than T_s. In spite of this, the microcontroller vendor suggests to update the registers of the digital PWM peripheral only in the next half carrier period (see Fig.3). It means that the voltage reference signals calculated before the negative peak are latched into the CR registers only at the negative peak and vice versa. It results in a constant T_s time delay in the control algorithm between the current sampling and the update of the duty ratios.

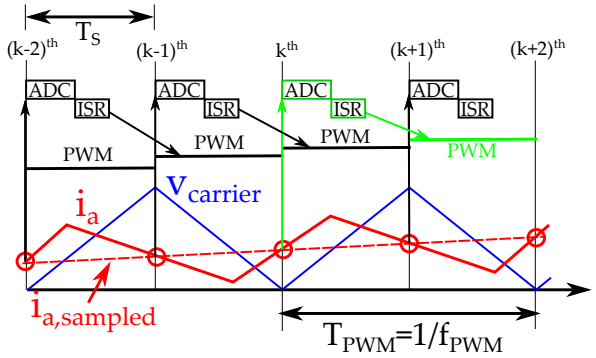

Fig. 3. Sequence of sampling, calculation and PWM update in a processor based drive system

B. Effect of discretization

At low F ratio the effect of model discretization magnifies, and some additional errors in the estimation can occur. According to our findings, one possible source of error can arise from the mismatch between the sampled current and sampled voltage values. Let us assume the estimator reads the current signal at the negativ peak of the carrier signal in the kth period (see Fig.3). Due to the delay in the PWM module, the value of the sampled current was caused by the applied voltage vector which was calculated during the $(k-2)^h$ period. If the estimator algorithm uses the value of the stator voltage vector calculated in the previous $(k-1)^{th}$ period, a mismatch occurs which can cause error or even instability in the estimator algorithm when the frequency ratio is a low number. This can be avoided by using the voltage vector which belongs to the actual current vector or by predicting the current vector in the next sampling instant.

Another problem, which is crucial at low F ratio, is the phase error between the real and estimated flux or BEMF vectors caused by the discretization and the delay. It can be avoided by adding a compensating angle during the rotation of the vectors. The compensating angle can be assumed to be ωT_s or $\omega_1 T_s$, however, depending on the loading conditions this value can change. Paper [3] introduces a controller, which calculates the value of the compensating angle using an integral type controller for MRAS observer.

V. Simulation Results

A detailed simulation analysis was carried out using Matlab/Simulink environment. The parameters of the machine with rated speed 18 000 rpm can be found in the appendix.

During the simulation the delays occuring in a microcontroller or DSP based system are also taken into consideration.

A. Flux observers

In this section, the parameter sensitivity analysis of the flux observer based on the stator current and the Gopinath estimator is performed. The parameters under the scope are the rotor resistance R_r and the mutual inductance L_m. The sampling f_s and the switching f_c frequency are also changed to demonstrate the effect of the $m_f = f_c/f_1$ and $F = f_s/f_1 = 2m_f$ ratios.

The simulation analysis was performed in open-loop and closed loop as well.

1) Open-loop operation: During this test the machine is supplied by its rated voltage at its rated fundamental frequency ($f_1 = 300$ Hz) and it is loaded by the rated torque.

To demonstrate and compare the performance of the flux observers the relative error in the estimation of the rotor flux amplitude and the error in the rotor flux angle estimation were calculated in steady state. The first one is calculated as $\Delta\Psi_r = \frac{|\Psi_{r,real} - \Psi_{r,est}|}{\Psi_{r,real}}$, while the error in the rotor flux angle estimation is obtained as $\varrho_{err} = |\varrho_{\Psi_r,real} - \varrho_{\Psi_r,est}|$.

Figure 4 summarizes the simulation results for parameter sensitivity in table form. As it can be seen the Gopinath estimator has a much better performance than the flux observer based on the stator current. It is less sensitive on the change in the parameters and estimates both the amplitude and the angle of the rotor flux with good accuracy even at low frequency ratios.

As it can be seen both estimator is more sensitive on the value of R_r. Based on 4, it is worth to point out that, the magnitude of the error is not the same for positive and negative changes in L_m and R_r parameters.

$R_{r,est}/R_r$	-30%		-20%		-10%		-5%		0		+5%		+10%		+20%		+30%	
	$\Delta\Psi_r$ [%]	ϱ_{err} [rad]	$\Delta\Psi_r$ [%]	ϱ_{err} [rad]	$\Delta\Psi_r$ [%]	ϱ_{err} [rad]	$\Delta\Psi_r$ [%]	ϱ_{err} [rad]	$\Delta\Psi_r$ [%]	ϱ_{err} [rad]	$\Delta\Psi_r$ [%]	ϱ_{err} [rad]	$\Delta\Psi_r$ [%]	ϱ_{err} [rad]	$\Delta\Psi_r$ [%]	ϱ_{err} [rad]	$\Delta\Psi_r$ [%]	ϱ_{err} [rad]
m_f=31	26.5	0.11	17.2	0.08	8.2	0.04	3.9	0.02	0.3	0.00	4.4	0.02	8.3	0.03	16.0	0.07	23.2	0.10
m_f=21	26.3	0.12	16.9	0.08	8.0	0.04	3.7	0.03	0.5	0.01	4.6	0.01	8.6	0.03	16.3	0.07	23.6	0.10
m_f=15	25.9	0.12	16.6	0.09	7.6	0.05	3.2	0.03	1.0	0.01	5.1	0.00	9.1	0.02	16.9	0.06	24.1	0.09
m_f=13	25.7	0.13	16.4	0.09	7.4	0.06	3.0	0.04	1.2	0.02	5.4	0.00	9.4	0.02	17.1	0.05	24.5	0.09
m_f=11	25.4	0.14	15.9	0.10	6.9	0.06	2.5	0.05	1.8	0.03	5.9	0.01	10.0	0.01	17.8	0.05	25.1	0.08
m_f=9	24.7	0.15	15.2	0.11	6.0	0.08	1.6	0.06	2.7	0.04	6.9	0.02	11.0	0.00	18.9	0.03	26.3	0.07

(a) Sensitivity of flux observer based on stator current to R_r parameter

$L_{m,est}/L_m$	-30%		-20%		-10%		-5%		0		+5%		+10%		+20%		+30%	
	$\Delta\Psi_r$ [%]	ϱ_{err} [rad]	$\Delta\Psi_r$ [%]	ϱ_{err} [rad]	$\Delta\Psi_r$ [%]	ϱ_{err} [rad]	$\Delta\Psi_r$ [%]	ϱ_{err} [rad]	$\Delta\Psi_r$ [%]	ϱ_{err} [rad]	$\Delta\Psi_r$ [%]	ϱ_{err} [rad]	$\Delta\Psi_r$ [%]	ϱ_{err} [rad]	$\Delta\Psi_r$ [%]	ϱ_{err} [rad]	$\Delta\Psi_r$ [%]	ϱ_{err} [rad]
m_f=31	8.5	0.14	4.8	0.08	2.0	0.04	0.8	0.02	0.3	0.00	1.2	0.02	2.0	0.04	3.5	0.06	4.7	0.09
m_f=21	8.2	0.14	4.5	0.08	1.7	0.03	0.5	0.01	0.5	0.01	1.5	0.02	2.3	0.04	3.8	0.07	5.0	0.09
m_f=15	7.8	0.13	4.1	0.07	1.2	0.03	0.1	0.00	1.0	0.01	1.9	0.03	2.8	0.05	4.2	0.08	5.4	0.10
m_f=13	7.6	0.12	3.9	0.07	1.0	0.02	0.2	0.00	1.2	0.02	2.2	0.04	3.0	0.05	4.5	0.08	5.7	0.10
m_f=11	7.1	0.12	3.4	0.06	0.5	0.01	0.7	0.01	1.8	0.03	2.7	0.04	3.6	0.06	5.0	0.09	6.2	0.11
m_f=9	6.2	0.10	2.5	0.05	0.4	0.00	1.6	0.02	2.7	0.04	3.6	0.06	4.5	0.07	6.0	0.10	7.2	0.12

(b) Sensitivity of flux observer based on stator current to L_m parameter

$R_{r,est}/R_r$	-30%		-20%		-10%		-5%		0		+5%		+10%		+20%		+30%	
	$\Delta\Psi_r$ [%]	ϱ_{err} [rad]	$\Delta\Psi_r$ [%]	ϱ_{err} [rad]	$\Delta\Psi_r$ [%]	ϱ_{err} [rad]	$\Delta\Psi_r$ [%]	ϱ_{err} [rad]	$\Delta\Psi_r$ [%]	ϱ_{err} [rad]	$\Delta\Psi_r$ [%]	ϱ_{err} [rad]	$\Delta\Psi_r$ [%]	ϱ_{err} [rad]	$\Delta\Psi_r$ [%]	ϱ_{err} [rad]	$\Delta\Psi_r$ [%]	ϱ_{err} [rad]
m_f=31	7.0	0.06	4.4	0.03	2.1	0.01	0.9	0.00	0.1	0.01	1.1	0.02	2.1	0.03	3.9	0.04	5.5	0.06
m_f=21	8.5	0.04	5.3	0.02	2.4	0.00	1.1	0.01	0.2	0.02	1.4	0.02	2.6	0.03	4.7	0.05	6.7	0.06
m_f=15	9.4	0.02	5.9	0.00	2.7	0.01	1.2	0.02	0.3	0.03	1.6	0.04	2.9	0.04	5.3	0.06	7.4	0.07
m_f=13	9.8	0.01	6.1	0.01	2.8	0.02	1.2	0.03	0.2	0.04	1.6	0.05	3.0	0.05	5.4	0.07	7.6	0.08
m_f=11	10.2	0.02	6.4	0.03	3.0	0.04	1.4	0.05	0.2	0.06	1.6	0.06	3.0	0.07	5.5	0.08	7.8	0.09
m_f=9	11.0	0.05	7.0	0.06	3.4	0.07	1.8	0.08	0.2	0.08	1.4	0.09	2.8	0.09	5.5	0.10	7.9	0.11

(c) Sensitivity of Gopinath flux estimator to R_r parameter

$L_{m,est}/L_m$	-30%		-20%		-10%		-5%		0		+5%		+10%		+20%		+30%	
	$\Delta\Psi_r$ [%]	ϱ_{err} [rad]	$\Delta\Psi_r$ [%]	ϱ_{err} [rad]	$\Delta\Psi_r$ [%]	ϱ_{err} [rad]	$\Delta\Psi_r$ [%]	ϱ_{err} [rad]	$\Delta\Psi_r$ [%]	ϱ_{err} [rad]	$\Delta\Psi_r$ [%]	ϱ_{err} [rad]	$\Delta\Psi_r$ [%]	ϱ_{err} [rad]	$\Delta\Psi_r$ [%]	ϱ_{err} [rad]	$\Delta\Psi_r$ [%]	ϱ_{err} [rad]
m_f=31	3.3	0.04	1.8	0.03	0.7	0.02	0.3	0.01	0.1	0.01	0.5	0.00	0.8	0.00	1.3	0.01	1.7	0.01
m_f=21	3.1	0.05	1.7	0.04	0.6	0.03	0.2	0.02	0.2	0.02	0.5	0.01	0.8	0.01	1.3	0.00	1.7	0.01
m_f=15	2.8	0.07	1.5	0.06	0.5	0.04	0.1	0.04	0.3	0.03	0.6	0.02	0.8	0.02	1.2	0.01	1.6	0.00
m_f=13	2.8	0.09	1.4	0.07	0.5	0.05	0.1	0.05	0.2	0.04	0.5	0.03	0.8	0.03	1.2	0.02	1.5	0.01
m_f=11	2.7	0.10	1.4	0.08	0.5	0.07	0.1	0.06	0.2	0.06	0.4	0.05	0.6	0.04	1.0	0.03	1.3	0.03
m_f=9	2.8	0.13	1.6	0.11	0.8	0.10	0.4	0.09	0.2	0.08	0.1	0.08	0.3	0.07	0.6	0.06	0.8	0.05

(d) Sensitivity of Gopinath estimator to L_m parameter

Fig. 4. Simulation results, sensitivity of flux observers at rated speed and at rated loading torque ($f_1 = 300$ Hz, $M_n = 1.6$ Nm)
Color code: Green (Good): $\Delta\Phi_r < 5\%$, $\varrho_{err} < 0.08$rad, Yellow (Moderate): $5\% \leq \Delta\Phi_r < 10\%$, 0.08rad$\leq \varrho_{err} <$ 0.15rad, Red (Bad): $10\% \leq \Delta\Phi_r$, 0.15rad$\leq \varrho_{err}$

2) Closed-loop operation: The performance of the flux observers was evaluated in closed loop as well. In this case the machine was controlled by Field Oriented Control method and the flux estimators provided the amplitude and the angle of the rotor flux.

Figure 5 presents the simulated time function of the mechanical speed and the electric torque in closed loop both when the flux observer based on stator current and when the Gopinath estimator was used. The reference speed was selected to be $\omega* = 1750$ rad/sec ($f_1 \approx 275$ Hz). The machine loading torque was changed suddenly in both direction. The sensitivity of the flux observer to parameter variation is also tested. Both the value of L_m and R_r, which is used in the estimator are changed in both directions.

Figure 5(a) presents the time function of ω and M when the switching frequency was selected to be $f_s = 3.6$ KHz ($m_f \approx 13$, $F \approx 26$). The value of the rotor resistance used in the estimation was suddenly change by 10% in both direction (see lower diagramm on Fig.5(a)). As it can be seen the vector control works properly for both flux observers. As it was demonstrated in the previous subsection, the flux observer based on the stator current is more sensitive on the value of R_r. If the rotor resistance used in the estimator is changed by 20% in the negative direction (see Fig.5(b)) the flux observer based on the stator current cannot provide correct results and the closed loop control becomes unstable. By using Gopinath estimator the system remains stable.

As it was shown previously, the estimators are less sensitive on change in the parameter L_m. Figure 5(c) presents the simulated Ω and M when the switching frequency is only 3 kHz ($m_f \approx 11, F \approx 22$) and the value of L_m used in the estimator is changed by 20% in both direction. The controller works properly in both cases.

B. Speed Estimators

1) Open-loop operation: During this test the machine is supplied by its rated voltage at its rated fundamental frequency ($f_1 = 300$ Hz).

It should be noted, the PLL-type estimator requires the magnitude of the actual rotor flux (the actual angle of the rotor flux is calculated by the algorithm). During the simulation study, it is provided by the Gopinath estimator.

Figure 6 presents the time function of the real and the estimated mechanical angular speed, when the loading torque as well as the value of R_r and L_m used in the estimation are changed suddenly when the switching frequency is only $f_c = 3.3$ kHz ($m_f \approx 11, F \approx 22$). The relative error in the speed estimation is calculated as $\frac{\omega - \omega_{est}}{\omega}$.

As it can be seen both the CB-MRAS and PLL-type speed estimator works properly and the error in the speed estimation is less than 1% even when the machine parameters used in the algorithm deviate from the real ones. Comparing the two methods, it can be seen the PLL has a slightly better performance.

2) Closed-loop operation: The performance of the speed estimators was evaluated in closed loop as well. In this case the machine was controlled by Field Oriented Control method and the estimators provided the mechanical speed, as well as the actual rotor flux angle.

Figure 7 presents the simulated time function of the mechanical speed and the electric torque in closed loop

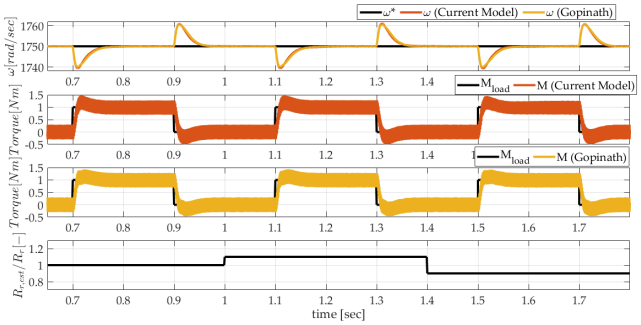

(a) Sensitivity on R_r, $f_s = 3.6$ KHz, $m_f \approx 13 (F \approx 26)$

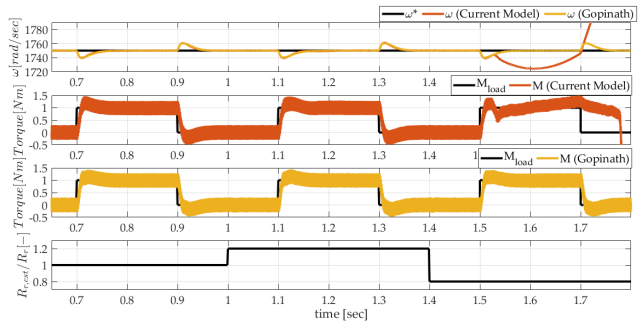

(b) Sensitivity on R_r, $f_s = 3.6$ KHz, $m_f \approx 13 (F \approx 26)$

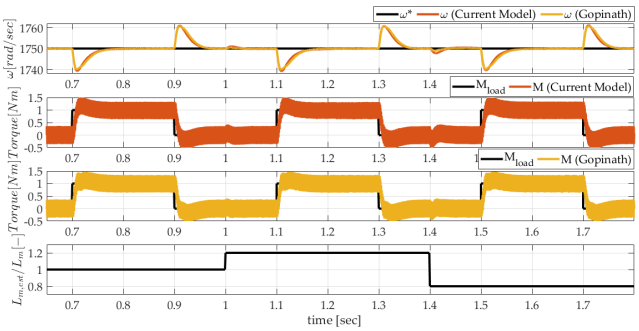

(c) Sensitivity on L_m,$f_s = 3$ KHz, $m_f \approx 11 (F \approx 22)$

Fig. 5. Simulation results, performance of flux observers in closed loop operation

using both speed estimator algorithms. The reference speed was selected again to be $\omega* = 1750$ rad/sec ($f_1 \approx 275$ Hz). The machine loading torque was changed suddenly in both directions. The sensitivity of the speed estimator to parameter variation is also tested. Both the value of L_m and R_r used in the estimator are changed suddenly in both direction.

As it can be seen the closed loop control has stable operation. The mechanical speed follows the reference speed, the error is around 1%. By comparing the performance of CB-MRAS and PLL-type speed estimators it can be seen the response of the PLL-type estimator became more oscillatory if there is a positive mismatch between the real and the estimated R_r value (see Fig.7(a)). Similarly to the flux observers, the speed estimators are less sensitive on the value of L_m (see Fig.7(b)).

VI. Conclusions

The paper focuses on high speed drives, where the low F ratio can be a source of possible error during the discretization of the estimator algorithms.

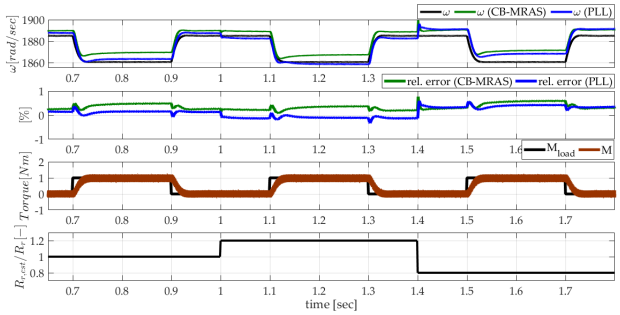

(a) Sensitivity on R_r, $f_s = 3.3$ KHz, $m_f \approx 11 (F \approx 22)$

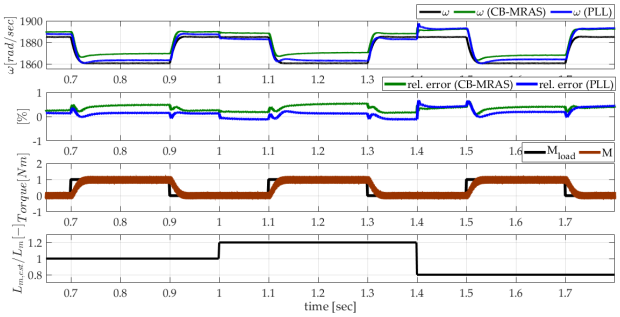

(b) Sensitivity on L_m, $f_s = 3.3$ KHz, $m_f \approx 11 (F \approx 22)$

Fig. 6. Simulation results, performance of speed estimators in open loop operation

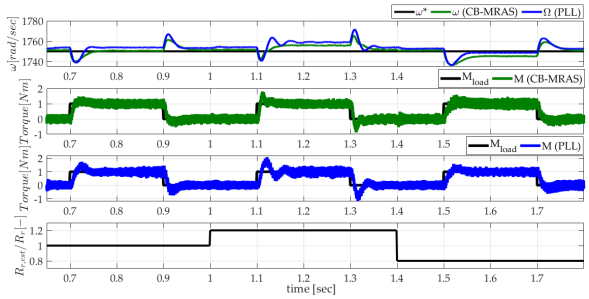

(a) Sensitivity on R_r, $f_s = 3.6$ KHz, $m_f \approx 13 (F \approx 26)$

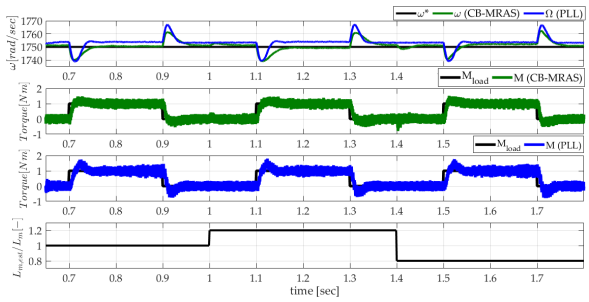

(b) Sensitivity on L_m, $f_s = 3.6$ KHz, $m_f \approx 13 (F \approx 26)$

Fig. 7. Simulation results, performance of speed estimators in closed loop operation

The paper introduces the theoretical background of the selected flux and speed estimator techniques. The discrete-time equations of each algorithm is derived by using Tustin approximation. The discrete form of each algorithm can be implemented by the recursive equations presented in this paper.

The performance of the algorithms both in open and closed loop is validated via numerical simulation using a high speed motor drive with a low sampling to fundamental frequency ratio.

Another paper will discuss the laboratory measurements with additional information on the practical implementation.

Appendix

The rated data and main parameters of the machine are: power: $P_N = 3$ kW, $U_{LL,RMS} = 380$V, $I_{N,RMS} = 7.7$A, $f_{1N} = 300$ Hz, $R_S = 1.125\Omega$, $R_R = 0.85\Omega$, $X_{LS} = 4.71\Omega$ and $X_{LR} = 2.63\Omega$, $X_m = 84.82\Omega$ (all reactance are at rated frequency), $p = 1$

References

[1] A. Tenconi, S. Vaschetto, and A. Vigliani, "Electrical machines for high-speed applications: Design considerations and tradeoffs," *IEEE Transactions on Industrial Electronics*, vol. 61, no. 6, pp. 3022–3029, June 2014.

[2] K. S. Kim and I. H. Kim, "Design of a discrete flux observer by the power series approximation," *Journal of Power Electronics*, vol. 11, no. 3, pp. 304–310, March 2011.

[3] D. Marcetic, I. Krcmar, M. Gecic, and P. Matic, "Discrete rotor flux and speed estimators for high-speed shaft-sensorless im drives," *Industrial Electronics, IEEE Transactions on*, vol. 61, no. 6, pp. 3099–3108, June 2014.

[4] B. Wang, Y. Zhao, Y. Yu, G. Wang, D. Xu, and Z. Dong, "Speed-sensorless induction machine control in the field-weakening region using discrete speed-adaptive full-order observer," *IEEE Transactions on Power Electronics*, vol. 31, no. 8, pp. 5759–5773, Aug 2016.

[5] T. O.-K. Mateusz Korzonek, "Application of different numerical integration methods for discrete mras-cc estimator of induction motor speed comparative study," in *IEEE PEMC 2018 18th International Conference on Power Electronics and Motion Control*, 2018, pp. 808–8013.

[6] N. T. West and R. D. Lorenz, "Digital implementation of stator and rotor flux-linkage observers and a stator-current observer for deadbeat direct torque control of induction machines," *IEEE Transactions on Industry Applications*, vol. 45, no. 2, pp. 729–736, March 2009.

[7] T. Orlowska-Kowalska and M. Dybkowski, "Stator-current-based mras estimator for a wide range speed-sensorless induction-motor drive," *IEEE Transactions on Industrial Electronics*, vol. 57, no. 4, pp. 1296–1308, April 2010.

[8] Y. B. Zbede, S. M. Gadoue, and D. J. Atkinson, "Model predictive mras estimator for sensorless induction motor drives," *IEEE Transactions on Industrial Electronics*, vol. 63, no. 6, pp. 3511–3521, June 2016.

[9] H. H. Vo, P. Brandstetter, and C. S. T. Dong, "Mras observers for speed estimation of induction motor with direct torque and flux control," in *AETA 2015: Recent Advances in Electrical Engineering and Related Sciences*. Springer, 2016, pp. 325–335.

[10] I. Krcmar, P. Matic, and D. Marcetic, "Discrete rotor flux estimator for high performance induction motor drives with low sampling to fundamental frequency ratio," *International Review of Electrical Engineering*, vol. 7, pp. 3804–3813, Aug 2012.

[11] J. O. K. C. Klarenbach, H. Schmirgel, "Design of fast and robust current controllers for servo drives based on space vector modulation," in *PCIM Europe 2011; International Exhibition and Conference for Power Electronics, Intelligent Motion, Renewable Energy and Energy Management*, 2011, pp. 182–188.

[12] S. N. Vukosavic, L. S. Peric, and E. Levi, "Ac current controller with error-free feedback acquisition system," *IEEE Transactions on Energy Conversion*, vol. 31, no. 1, pp. 381–391, March 2016.